Climate
of the Past

Decadal resolution record of Oman upwelling indicates solar forcing of the Indian summer monsoon (9–6 ka)

Philipp M. Munz[1,2], Stephan Steinke[3], Anna Böll[4], Andreas Lückge[5], Jeroen Groeneveld[6], Michal Kucera[6], and Hartmut Schulz[2]

[1]Senckenberg Centre for Human Evolution and Palaeoenvironment (HEP) at the University of Tübingen, Hölderlinstr. 12, 72074 Tübingen, Germany
[2]Department of Geosciences, University of Tübingen, Hölderlinstr. 12, 72074 Tübingen, Germany
[3]Department of Geological Oceanography, Xiamen University, Xiping Building, Xiang'an South Road, Xiamen 361102, China
[4]Institute of Geology, University of Hamburg, Bundesstr. 55, 20146 Hamburg, Germany
[5]Bundesanstalt für Geowissenschaften und Rohstoffe (BGR), Stilleweg 2, 30655 Hannover, Germany
[6]MARUM – Center for Marine Environmental Sciences, Germany, Leobener Str., 28359 Bremen, Germany

Correspondence to: Philipp M. Munz (philipp.munz@uni-tuebingen.de)

Abstract. The Indian summer monsoon (ISM) is an important conveyor in the ocean–atmosphere coupled system on a trans-regional scale. Here we present a study of a sediment core from the northern Oman margin, revealing early to mid-Holocene ISM conditions on a near-20-year resolution. We assess multiple independent proxies indicative of sea surface temperatures (SSTs) during the upwelling season together with bottom-water conditions. We use geochemical parameters, transfer functions of planktic foraminiferal assemblages and Mg / Ca palaeothermometry, and find evidence corroborating previous studies showing that upwelling intensity varies significantly in coherence with solar sunspot cycles. The dominant ∼ 80–90-year Gleissberg cycle apparently also affected bottom-water oxygen conditions. Although the interval from 8.4 to 5.8 ka BP is relatively short, the gradually decreasing trend in summer monsoon conditions was interrupted by short events of intensified ISM conditions. Results from both independent SST proxies are linked to phases of weaker oxygen minimum zone (OMZ) conditions and enhanced carbonate preservation. This indicates that atmospheric forcing was intimately linked to bottom-water properties and state of the OMZ on decadal timescales.

1 Introduction

The Indian summer monsoon (ISM) is the dominant driver for intraseasonal changes of wind directions and precipitation patterns in one of the world's most densely populated regions in southern Asia. For the agricultural development and economic prosperity of the region, it is therefore vital to assess the variability in the monsoon system on societally relevant decadal to centennial timescales. This might help to better understand how potential driving forces might be controlling ISM variability and how it might develop under future climate scenarios. To precisely determine possible changes under climatic conditions in response to anthropogenic impact, it is vital to understand how ISM variability is modulated on societally relevant decadal to centennial timescales. In comparison to modern times, the early to mid-Holocene is marked by different orbital configurations, affecting Northern Hemisphere insolation (A. L. Berger, 1978) and monsoon circulations (Kutzbach and Street-Perrott, 1985). This period was marked by a steep decline in solar insolation changes, whilst climatic conditions were largely unaffected by human-induced greenhouse gas emissions. Furthermore, climatic conditions during the early to mid-Holocene have been attributed to cultural and societal turnover in Africa
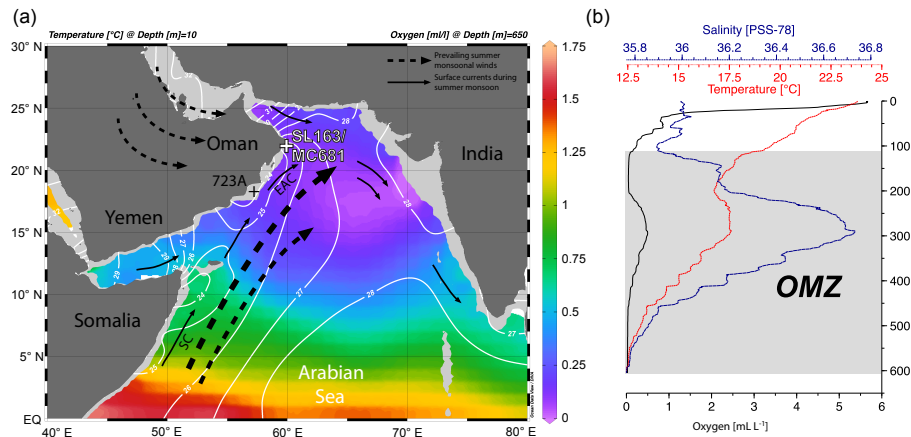
Figure 1. (a) Map of the Arabian Sea, showing the location of gravity core SL163 and multicorer MC681 (white cross) at the northern Oman margin (21°55.97′ N, 059°48.15′ E) in 650 m water depth, as well as Integrated Ocean Drilling Program (IODP) core 723A (black cross) studied by Gupta et al. (2005). Black arrows show the schematic pathways of major currents (solid lines; SC is Somali Current and EAC is East Arabian Current) and near-surface winds (stippled lines) during the summer monsoon. White contour lines refer to the summer (July to September) sea surface temperature (SST) in 10 m water depth. Colour shading indicates oxygen concentration (mL L^{-1}) in 650 m water depth, indicating a strong oxygen deficiency in the modern depth of the sampled sediment core. SST (Locarnini et al., 2010) and oxygen concentration (Garcia et al., 2010) are from World Ocean Atlas 2009. Panel **(b)** shows the depth profile of oceanographic data (salinity, temperature and oxygen) measured during cruise M74/1b at the station of core SL163. Grey shading refers to the location of the modern oxygen minimum zone (OMZ). A subsurface salinity maximum in 200–400 m water depth indicates the location of Persian Gulf Water (PGW). The map was created using the software ODV ver. 4.7.4 (Schlitzer, 2015).

(Kuper and Kröpelin, 2006) and Mesopotamia (Kennett and Kennett, 2007).

Monsoonal winds develop when summer (July to September) heating over the continent forms a low-pressure zone over continental Asia, which then interacts with the high-pressure zone over the southern Indian Ocean and drives strong, moisture-laden southwesterly winds. Along the eastern coast off Somalia and Oman, the alongshore winds induce coastal upwelling of cold and nutrient-rich deeper water layers, which cool surface water temperatures and fuel biological productivity within the euphotic zone (Findlater, 1969; Wyrtki, 1973). Below the photic zone, remineralisation of sinking organic matter consumes oxygen, which leads, in combination with the lateral supply of low-oxygenated intermediate water masses (You and Tomczak, 1993), to the formation of a pronounced mid-depth oxygen minimum zone (OMZ). Upwelling and OMZ intensity, together with the biological uptake and release of carbon dioxide (CO_2), nitrous oxide (N_2O) and other greenhouse gases from and into the atmosphere (Farías et al., 2009; Paulmier et al., 2011; Ward et al., 2009), play a critical role in the global climate system.

Quantitative reconstructions of upwelling intensity have the advantage of being directly related to wind strength and thus ISM intensity (Murtugudde et al., 2007). Numerous studies attempted to quantitatively reconstruct sea surface temperatures (SSTs) in the northwestern Arabian Sea to study changes in upwelling and thus ISM intensity (Emeis et al., 1995; Clemens et al., 1991; Naidu and Malmgren, 1996; Dahl and Oppo, 2006; Huguet et al., 2006; Anand

et al., 2008; Godad et al., 2011). Accordingly, ISM variations are modulated by Northern Hemisphere summer insolation changes controlled by orbital parameters of the earth's precessional cycle. However, previous reconstructions of Arabian Sea SST did not resolve variations on societally relevant decadal to centennial timescales. Here, we present a high-resolution study of early to mid-Holocene ISM variability based on a multi-proxy study comprising of SST fluctuations and OMZ intensity. Reconstructions are based on a comparison of Mg / Ca measurements of the upwelling-related species *Globigerina bulloides* and on transfer functions based on planktic foraminiferal (PF) census counts. To this end we first evaluate species response to potential ecological driving parameters and convert fossil assemblage counts to summer SST using a regionally validated transfer function (Munz et al., 2015). We test the ecological importance and statistical significance of the reconstructions and evaluate summer SST variability in comparison to other proxy records. We further assess the influence of surface parameters, upwelling SST and primary productivity on variations in OMZ intensity and deep-water carbonate preservation.

2 Modern oceanographic setting

Modern hydrographic conditions in the Arabian Sea are strongly dominated by the seasonal monsoon cycle. During boreal summer (June–September), strong southwestern monsoonal winds drive surface currents in the western Arabian

Sea (Fig. 1), namely the Somali Current (SC) and as its northward extension the East Arabian Current (EAC), promoting an overall anti-cyclonic circulation pattern (Shetye et al., 1994; Tomczak and Godfrey, 1994). The alongshore surface currents induce an offshore-directed deflection of surface waters and an upwelling of deeper, cold and nutrient-rich subsurface waters through the process of Ekman pumping. During boreal winter (December–March), weaker, dry and cold northeasterly winds (IWM, Indian winter monsoon) lead to increased surface water cooling and evaporation, especially in the northeastern part of the basin, where the IWM enables deep convective mixing and a second productivity peak during winter (Madhupratap et al., 1996; Schulz et al., 2002; Munz et al., 2015, 2016). Enhanced nutrient availability during summer upwelling nourishes primary productivity within the photic zone near the Somali and Omani coasts. This promotes OMZ conditions at intermediate water levels ($\sim$ 100–1000 m; Fig. 1).

The water masses in the Arabian Sea are derived from several major sources. High evaporation leads to highly saline surface water, which is therefore named Arabian Sea High-Salinity Water (ASHSW) (Shetye et al., 1994; Prasanna Kumar and Prasad, 1999). Thermocline waters are mainly sourced from an intermediate water mass (500–1500 m water depth) that originates in the central Indian Ocean (Indian Ocean Central Water, IOCW) as a mixture of Antarctic Intermediate Water (AAIW) and Indonesian Intermediate Water (IIW) (Emery and Meincke, 1986; You, 1998). Although intermediate waters have a relatively low pre-formed oxygen saturation when they arrive in the Arabian Sea (0.07–0.52 mL L^{-1}), they exert a strong influence on the OMZ of the Arabian Sea. Additionally, intermediate waters are sourced from the inflow of highly saline waters forming through excess evaporation over precipitation in the Persian Gulf and Red Sea. This leads to the formation of high salinity subsurface waters (35.5–36.8 psu) and subduction under less-saline waters after entering the Arabian Sea. The Persian Gulf Water (PGW) shows a pronounced salinity maximum at 200–400 m water depth, whereas the Red Sea Water (RSW) has an equilibrium depth of 500 m at its maximum northward extent at $\sim$ 18° N (Shetye et al., 1994). Although the PGW is a relatively young water mass and originates from a closer source region compared to the other intermediate water masses, the high-salinity tongue of the modern PGW increases the oxygen concentration at mid-depth by less than 0.5 mL L^{-1} (Fig. 1).

3 Material and methods

3.1 Samples and chronology

During RV *Meteor* cruise M74 on Leg 1b in September 2007 (Bohrmann et al., 2010), piston core SL163 recovered the uppermost 955 cm of the sedimentary sequence from 650 m water depth within the central part of the present-day OMZ (Fig. 1) at the northern Oman margin (21°55.97′ N, 059°48.15′ E). Multicorer MC681 recovered the undisturbed uppermost 53 cm of near-surface sediments at the same position. The sedimentary sequence from the intervals 1–56 cm of core SL163 and 1–53 cm of MC681 is considerably different from the topmost 1 cm and the deeper intervals of SL163. From smear slide analysis and scanning electron microscopy this deposition can be described as faintly bioturbated, olive-brown organic-rich diatomaceous nannofossil silty clay. The uppermost 1 cm from both cores as well as the deposition below 56 cm of SL163 is described as olive foraminiferal nannofossil ooze. We did not find any evidence for interruptions of the stratigraphical record in the form of slumps, turbidites, erosional surfaces or phosphorites below the unconformity at 56 cm core depth. In this study, we focus only on samples from the foraminiferal nannofossil ooze between 56 and 400 cm of SL163 and the core top (0–1 cm) of MC681 and therefore assume that the record we present here is deposited homogeneously and undisturbed.

Core SL163 was sampled in continuous 1–2.5 cm intervals. The age model of core SL163 and the core top sample of MC681 is based on 14 accelerator mass spectrometry ^{14}C datings (Table 1), measured at Beta Analytic, Miami, USA, and the Leibniz Laboratory in Kiel, Germany. Datings of core SL163 were mostly based on a monospecific analysis of handpicked individuals of *Neogloboquadrina dutertrei* (Table 1). This species is commonly known to thrive at thermocline depths (e.g. Fairbanks et al., 1982), but in the western Arabian Sea it shows a relatively shallow habitat within the upper 35 m of the water column (Peeters and Brummer, 2002). For two samples (52.5 and 58.5 cm) with insufficient foraminiferal carbonate content, the bulk organic fraction was dated. To avoid a potential bias introduced by dating different organic compounds that might have been produced during different seasons or within different water masses, the core top sample of MC681 was sampled twice using mixed planktic foraminifera and bulk organic fraction. Both analyses yielded comparable results (Table 1), indicating a similar synthesis and general comparability of both dating methods.

Radiocarbon dates were calibrated to calendar years using the Marine13 calibration curve (Reimer et al., 2013) within the program clam ver. 2.2 (Blaauw, 2010) for the statistical software environment R ver. 3.2.1 (R Core Team, 2015). We assume a regional reservoir correction of $\Delta R = 231 \pm 31$ years, which is the weighted mean of the four closest (maximum distance $\sim$ 700 km) ΔR determination points (Southon et al., 2002; von Rad et al., 1999) from the 14CHRONO Marine Reservoir Database (http://calib.org/marine/). Added to the global marine reservoir age of 400 years, this correction factor is consistent with the recent age of our undisturbed core top sample of MC681 (Table 1). An age–depth model was then built for SL163 using a smooth spline regression with a mixed-effect model (10 000 iterations) within clam.

Table 1. Samples for radiocarbon dating with the organic compound used, dating results and calibrated ages using the Marine13 calibration curve (Reimer et al., 2013), and a reservoir correction of $\Delta R = 231 \pm 31$ years. Analyses were conducted at Beta Analytic in Miami, FL, USA (Beta), and the Leibniz Laboratory in Kiel, Germany (KIA).

Lab code	Core	Sample type	Depth (cm)	Conventional ^{14}C age (years)	Error ±	δ^{13}C (‰)	Cal. min (95 %)	Cal. max (95 %)
Beta342813	MC681	mixed PF	1	650	30	−2.4		
Beta342812	MC681	bulk org.	1	630	30	−20.4		
Beta346603	SL163	bulk org.	52.5	2100	30	−19.4	1329	1505
Beta346604	SL163	bulk org.	58.5	5740	30	−19.3	5788	5973
KIA47119	SL163	*N. dutertrei*	77.75	5760	30	+0.24	5841	5987
Beta319751	SL163	*N. dutertrei*	141.25	5990	30	−0.5	6095	6266
Beta319752	SL163	*N. dutertrei*	193.75	6350	40	+0.5	6436	6646
KIA47120	SL163	*N. dutertrei*	252.75	6715	35	+0.48	6878	7114
Beta319753	SL163	*N. dutertrei*	278.75	6670	40	+0.8	6790	7043
Beta319754	SL163	*N. dutertrei*	295.0	7030	40	+0.3	7246	7407
Beta319755	SL163	*N. dutertrei*	326.25	6990	40	+0.4	7193	7386
KIA47121	SL163	*N. dutertrei*	353.75	7420	40	+1.59	7568	7737
KIA47122	SL163	*N. dutertrei*	392.5	8090	40	+1.42	8211	8396
Beta319756	SL163	*N. dutertrei*	395.0	8090	40	+0.8	8211	8396
Beta342816	SL163	*N. dutertrei*	417.5	8500	40	−0.4	8647	8957

Mixed PF = mixed planktic foraminifera. Bulk org. = bulk organic fraction.

3.2 Planktic foraminiferal faunal analyses and transfer function approach

Samples were freeze-dried, washed with tap water over a 63 µm screen, oven-dried at 40 °C, and dry-sieved into the size fractions 150–250, 250–315 and >315 µm. PF were identified according to the taxonomic framework of Hemleben et al. (1989), Bé (1967), and Bé and Hutson (1977). Following the procedure of Pflaumann et al. (1996), PF counts were conducted on a sub-split of each size fraction that contained a minimum of 100 PF individuals, yielding a summed fraction (>150 µm) to contain >300 identified PF individuals. Relative species abundances were calculated on the summed fraction >150 µm after multiplying each size fraction with the respective split factor. To evaluate the secondary influence of calcite dissolution, we calculated fragmentation indices following Le and Shackleton (1992).

Quantitative reconstructions from PF faunal abundances were based on a modern calibration dataset of $n = 603$ surface samples spanning the Indian Ocean from 30° S to 25° N and 33 to 119° E recently compiled by Munz et al. (2015). To enhance the signal-to-noise ratio, rare species with < 0.5 % average abundance were removed from the calibration dataset prior to further analyses (Kucera et al., 2005), which resulted in the exclusion of 16 rare species out of 33 taxa. The dataset was then further subsampled to contain only samples most similar to the fossil assemblages of core SL163. This removes noisy effects introduced by modern samples covering ecological conditions outside the range of the fossil samples (Kucera et al., 2005). We followed the approach presented in Munz et al. (2015) and restricted the calibration dataset to samples that had the same range along the first and second axes of a joint principal component analysis together with the fossil dataset (using square-root-transformed species abundances to dampen the effect of a few dominant taxa). The resulting subsampled dataset used for further analyses contained $n = 96$ modern surface samples (Fig. 2).

Environmental gradient analysis was then carried out on the 96 subsampled calibration samples using the package vegan ver. 2.3-1 (Oksanen et al., 2015) for R. An initial detrended correspondence analysis (DCA) revealed a short gradient length (0.75 for the longest gradient on DCA axis 1), suggesting an ordination method based on linear species response (Birks, 1998). Redundancy analysis (RDA) was therefore chosen for the construction of an ordination model to examine species response to several potential controlling environmental gradients. Because of the extreme seasonality of surface water productivity owing to the monsoonal circulation, four different approaches were used to assess modern productivity values. Net primary productivity estimates from the vertically generalized production model (VGPM), the *Eppley*-VGPM and the carbon-based productivity model (CbPM) were accessed through the Ocean Productivity Home Page (http://www.science.oregonstate.edu/ocean.productivity/). Satellite-derived chlorophyll α measurements of SeaWiFS and Aqua MODIS sensors averaged over the period 1998–2010 were obtained from NASA Ocean Biology (http://oceancolor.gsfc.nasa.gov/cms/). Sea surface salinity (SSS) and SST were extracted from the 10 m depth level of the World Ocean Atlas 1998 (Conkright et al., 1998).
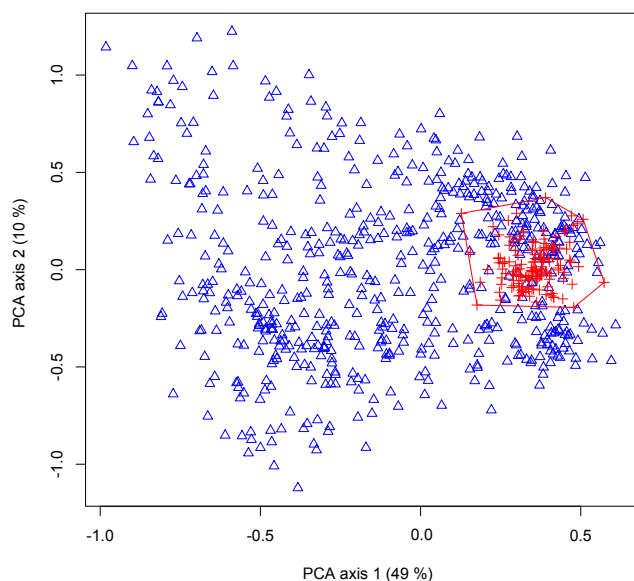
Figure 2. Scatterplot of the joint principal component analysis (PCA) of $n = 603$ modern calibration samples (blue triangles) and fossil downcore samples of SL163 (red crosses). The variance of the first and second PCA axes is indicated. $N = 96$ modern samples within the red polygon are most similar to the fossil samples along the first and second PCA axes, and were used for the calibration of transfer functions.

Transfer function analysis and statistical significance tests of the reconstructions were performed with the R packages rioja ver. 0.9-5 (Juggins, 2015) and palaeoSig ver. 1.1-3 (Telford, 2015). We used two common techniques for palaeoenvironmental reconstructions, the Imbrie–Kipp method (IK) (Imbrie and Kipp, 1971) and weighted-averaging partial-least-squares (WA-PLS) regression (ter Braak and Juggins, 1993), to reconstruct SST from the fossil samples. The number of factors to extract for IK was based on the Kaiser–Guttman criterion, the parallel analysis after Horn (1965) and the analysis of optimal coordinates (reviewed by Courtney and Gordon, 2013). WA-PLS model complexity was evaluated from the model of lowest root mean square error of prediction (RMSEP) using bootstrapping cross validation ($n = 999$ cycles).

3.3 Mg / Ca analyses and palaeothermometry of *G. bulloides*

For Mg / Ca analyses, approximately 30 individuals of *G. bulloides* were picked from the size fraction 250–315 µm, gently crushed between two glass plates under the microscope to open the chambers and cleaned following the protocol of Barker et al. (2003). Trace elemental measurements were performed with an inductively coupled plasma optical emission spectrometer (ICP-OES) using an Agilent Technologies 700 series with autosampler ASX-520 Cetac and micro-nebulizer at the MARUM Center for Marine Envi-

ronmental Sciences, University of Bremen, Germany. Precision of ICP-OES measurements was determined using an in-house standard with a Mg / Ca ratio of 2.93 mmol mol^{-1} after every five samples. The average relative standard deviation from $n = 55$ measurements was 0.155 % ($1\sigma = 0.005$). As a standard reference material, we analysed the international limestone standard ECRM752-1 with an Mg / Ca ratio of 3.75 mmol mol^{-1} (Greaves et al., 2008) prior to every batch of 50 samples. The average of Mg / Ca values over all ECRM752-1 measurements was 3.714 ($n = 8$; $1\sigma = 0.041$). Three replicate measurements of every sample were used to estimate analytical precision and yielded an average relative standard deviation of 0.068 % ($n = 234$ samples, $1\sigma = 0.004$). To estimate SST from Mg / Ca we used the species-specific calibration equation $T = 1/0.102 \times LN(\text{Mg} / \text{Ca}/0.528)$ published by Elderfield and Ganssen (2000) for *G. bulloides*. This Mg / Ca–temperature relationship was previously used for calibrating Mg / Ca measurements of *G. bulloides* in the Arabian Sea (Anand et al., 2008; Ganssen et al., 2011). Reconstruction errors were estimated using the error propagation approach of Mohtadi et al. (2014).

Samples were screened for potential contamination by iron–manganese coatings and clay minerals not successfully removed by the cleaning technique (Barker et al., 2003). Out of 142 samples, 10 showed Fe / Ca or Mn / Ca values of more than 0.1 mmol mol^{-1} and were excluded prior to further analyses. No correlations exist between Mg / Ca and element / Al ratios of Al / Ca ($r = 0.06$) and Fe / Ca ($r = 0.16$) and only weak correlations for Mn / Ca ($r = 0.36$). Palaeotemperature estimates based on trace elemental concentrations in foraminiferal calcite can potentially suffer from post-depositional dissolution and preferential removal of more solution-susceptible Mg-rich calcite (e.g. Brown and Elderfield, 1996; Dekens et al., 2002). Pteropod concentration was always > 0, except for 11 samples where they were likely diluted by a high concentration of foraminiferal shells. The persistent presence of aragonite indicates that selective dissolution could not affect Mg / Ca ratios, as planktic foraminifera build their shells from calcite, the more dissolution resistant polymorph of calcium carbonate compared to aragonite.

3.4 Bulk geochemical analyses

Bulk geochemical analyses of the sediment were performed on average every 5 cm with X-ray fluorescence (XRF). Concentrations of manganese (Mn) and vanadium (V) were quantitatively analysed as an indicator for bottom-water redox conditions and state of the OMZ. After fusion of the samples with lithium metaborate at 1200 °C for 20 min (sample/LiBO$_2$ = 1/5), samples were measured using Philips PW 2400 and PW 1480 wavelength dispersive spectrometers at the Federal Institute for Geosciences and Natural Resources, Hannover, Germany. Instrumental preci-

sion of the results was controlled with certified reference materials (CRM) (i.e. BCR, Community Bureau of Reference, Brussels). The precision for major elements was generally better than ± 0.5 % and better than 5 % for trace elements. To decipher a possible secondary alteration of the geochemical composition, the values were expressed as enrichment relative to the detrital background, or average shale, as expressed by Wedepohl (1971) and Wedepohl et al. (1991). Accordingly, it is calculated as the element / Al ratio of the sample divided by the element / Al ratio of average shale. Hence, element / Al ratio and enrichment factor are co-varying, with a factor > 1 indicating enrichment and < 1 indicating depletion relative to the detrital background.

Biogenic opal was determined photometrically after wet alkaline extraction of biogenic silica (BSi) using a modification of the DeMaster method (DeMaster, 1981). About 30 g of dry sediment per sample was digested in 40 mL of 1 % sodium carbonate solution (Na_2CO_3) in a shaking bath at 85 °C. After treatment with 0.021 M HCl, the neutralised supernatant was analysed after 3, 4, and 5 h and the amount of BSi was estimated from the linear intercept through the time course aliquots. Slope correction was used to prevent an overestimation of BSi by dissolution of clay minerals at low BSi concentrations (Conley, 1998). Biogenic opal was then determined by multiplying the BSi concentrations with a factor of 2.4. Duplicate measurements revealed a mean standard deviation of 0.13 %.

3.5 Spectral analyses

Spectral analyses of the proxy records from planktic foraminiferal transfer functions, Mg / Ca SST, and OMZ intensity with the multi-taper method (MTM; Mann and Lees, 1996) were computed with the SpectraWorks software kSpectra© ver. 3.4.5 and a red noise null hypothesis (Ghil et al., 2002) using the default setting of $p = 2$ and $K = 3$ tapers. A Gaussian band-pass filter was used to reveal the signature of the dominant cycles in the data. After resampling the time series to the average sampling rate, filtering was carried out using the software program AnalySeries ver. 2.0.8 (Paillard et al., 1996). A cross wavelet transform (XWT; Grindsted et al., 2004) of both temperature proxy time series was calculated with the bi-wavelet package ver. 0.17.10 for R. MTM and XWT analyses were conducted on trend-removed time series interpolated to regular average sample spacings using piecewise cubic polynomial interpolation (function "pchip" of the signal package ver. 0.7–6 for R). To estimate a linear relationship of the low-frequency signals between the differently spaced time series, a new common time axis was produced where signals were consecutively averaged into 60-year bins with a 20-year overlap.
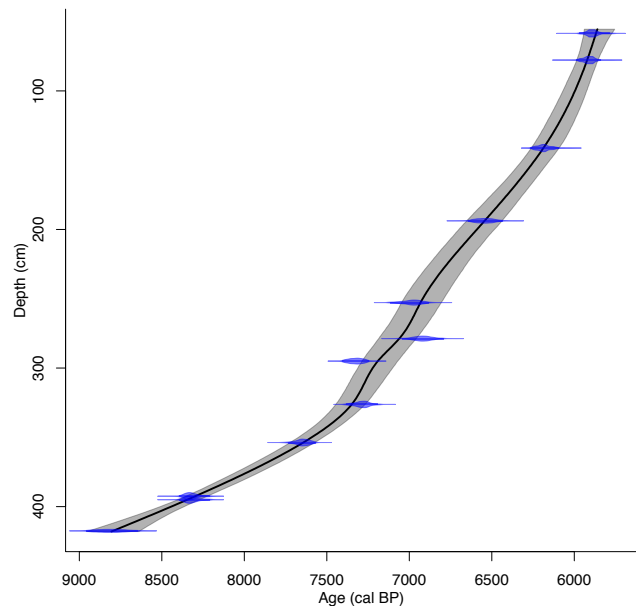

Figure 3. Age–depth relationship of the early to mid-Holocene section of core SL163 (55–400 cm). Blue areas indicate the conventional ^{14}C-calibrated ages; the black line indicates the interpolation between the dated samples using a smooth spline fit and the 95 % confidence level (grey shading).

4 Results

4.1 Age control

The 1–2.5 cm sample spacing yielded an average temporal sampling distance of ~ 19 years over the entire interval. The sample spacing fluctuates between < 10 years in the upper 50 cm of the core and close to 50 years in the lowermost 15 cm of the core. The sharp lithofacies change above the studied interval at 56 cm core depth is marked by a sedimentation hiatus of ~ 3600 years (Table 1). Based on the accumulation rates above and below the unconformity, this corresponds to a thickness of the missing sedimentary sequence of ~ 1.5 m. The diatomaceous ooze above the unconformity at 56 cm core depth of SL163 showed an excursive increase in the sedimentary water content of < 17 %. One possible reason for the sedimentation hiatus might thus be gravitational instability due to the high water content of the organic-rich diatomaceous silty clay deposited at the steeply inclined northern Oman margin. However, further discussion of this issue is beyond the scope of this study and will be presented elsewhere.

We observed two samples where the age–depth relationship was reversed within the lower half of the core (Fig. 3). However, the maximum age deviation is lower than the 2σ probability of both dating points, enabling the fit of a smooth spline model with continuous deposition rates and continuously increasing ages. As we did not find any indications of interruptions or other inconsistencies of the sedimenta-

tion within the studied interval, we are confident that our age model represents a continuous deposition. Instead, we assume the offset to be either the result of changing water mass ages due to changing upwelling intensities, as it was shown for the Peruvian upwelling (Fontugne et al., 2004), or due to mixing by bioturbation.

4.2 PF faunal analyses of core SL163 and palaeothermometry

A total of 29 PF morphospecies were identified in core SL163, whereof six species showed a total average abundance of > 5 % (Fig. 4). The overall PF fauna is dominated by *Globigerina bulloides* (39.2 %), followed by *Globigerinita glutinata* (11.5 %), *Globigerinoides ruber* (11.2 %), *Globigerina falconensis* (9.2 %), *Globigerinoides sacculifer* (8.3 %) and *Globigerinella siphonifera* (7.4 %). Core top studies (Bé and Hutson, 1977; Hutson and Prell, 1980; Prell and Curry, 1981), plankton tow casts (Peeters and Brummer, 2002) and sediment trap studies (Curry et al., 1992; Conan et al., 2002; Conan and Brummer, 2000; Mohan et al., 2006) in the Arabian Sea indicate that *G. bulloides* is the dominant species during upwelling season. Relative abundances of *G. bulloides* were used in a number of studies to express upwelling and ISM intensity (Naidu and Malmgren, 1996; Anderson et al., 2002; Gupta et al., 2005). The high numbers of *G. bulloides* throughout the studied interval of core SL163 suggest highly elevated primary productivity during the early to mid-Holocene summer upwelling at this station.

Modern surface water properties and plankton productivity at the northern Oman margin are dominated by the seasonal upwelling during boreal summer. Because PF assemblages are dominated by species produced during the upwelling season (Curry et al., 1992), we investigated the environmental control on the PF fauna during summer (July to September; J–A–S). RDA results indicate, that summer SST correlates best with the first RDA axis and is the strongest determinant in the explanation of PF assemblages among the investigated parameters (Table 2). Transfer functions were therefore calibrated to summer SST.

The three methods used for determining the factor numbers to retain for the IK transfer function approach suggested a number of $n = 4$ factors. For WA-PLS, a two-component model showed the best model performance ($r^2 = 0.65$) and lowest cross-validated error estimates (RMSEP = $0.95\,°C$). Performance estimates for both methods are given in Table 3. Statistical significance of the reconstructions was tested using a novel method of random forest reconstructions (Telford and Birks, 2011). The analysis shows that summer SST can be reconstructed from fossil PF assemblages of core SL163 with a high statistical significance (Table 3; Fig. 5). Reconstructed summer SST from both techniques (IK and WA-PLS) show a high linearity ($r = 0.82$; $p < 2.2 \times 10^{-16}$), indicating a low model-specific bias (Kucera et al., 2005). The resulting consensus of reconstructed summer SSTs from the
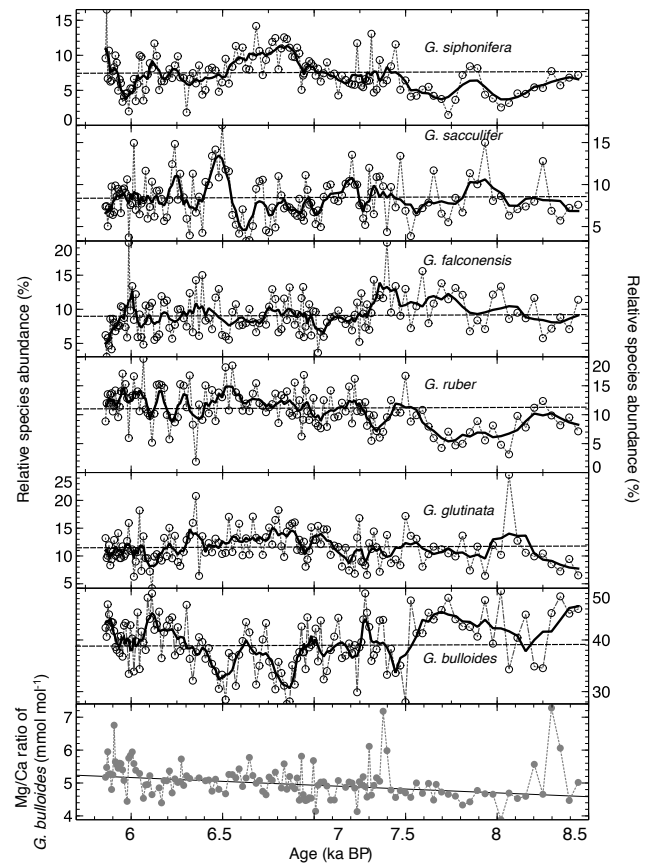

Figure 4. Time series of the six most common planktic foraminiferal species (> 5 % average abundance) and Mg / Ca measurements of *G. bulloides* from the studied interval in core SL163. Dashed lines are the real data; thick solid lines give the 3 pt running average.

transfer function techniques ranges between 23.3 and 25.8 °C (Fig. 6b). Compared to modern summer (J–A–S) SST (10 m depth interval), which is 25.8 °C at this station (Conkright et al., 1998), reconstructed early to mid-Holocene summer SSTs are thus < 2.5 °C colder.

Measured Mg / Ca values range between 3.9 and 7.3 mmol mol^{-1} (Fig. 4), corresponding to water temperatures ranging from 19.6 to 25.7 °C. The Mg / Ca value of 6.66 mmol mol^{-1} of the modern core top sample at this station (MC681) yields SST estimates ($T = 24.85\,°C$) close to modern summer SST of the upper 50 m of the water column (WOA1998 = 24.81 °C), indicating that the calibration equation of Elderfield and Ganssen (2000) is applicable to the Mg / Ca temperature dependence of *G. bulloides* at the northern Oman margin. Error propagation (Mohtadi et al., 2014) yields an average propagating 1σ error of 0.89 °C. We are aware of a potential bias introduced by a genotype-specific fractionation of Mg / Ca ratios, which was recently shown to occur between two species of *G. bulloides* that prefer warm water (type I) and cool water (type II) in the Arabian Sea

Table 2. Results of the redundancy analysis of the adjusted calibration dataset. Highest correlation with RDA1 axis and highest explanation of the PF assemblage variance (bold numbers) is shown by temperature (SST).

	RDA1	RDA2	RDA3	Captured variance of species data	Proportion (%)
Eigenvalue	1.763	0.185	0.097		
Cumulative proportion of variance explained (%)	35.9	39.6	41.6		
Correlation					
Temperature	**−0.93**	−0.07	0.15	1.55	**31.5**
Salinity	−0.87	0.47	−0.05	0.24	5.0
Eppley-VGPM	0.33	0.75	0.26	0.19	4.0
uCbPM	−0.02	−0.65	0.32	0.07	1.5
Chlorophyll α	0.39	0.36	−0.18	0.05	1.0

VGPM = vertical generalized production models. uCbPM = updated carbon-based production model.

Table 3. Cross-validated root mean square error of prediction (RMSEP) as absolute values and relative to the range of the target variable, as well as the coefficient of determination. The results of the significance analysis after Telford and Birks (2011) from both transfer function methods are given; p indicates the statistical significance against the null distribution of 999 random reconstructions.

	RMSEP	RMSEP (% of target range)	R^2	SST $p =$	*Eppley*-VGPM $p =$
Imbrie–Kipp	0.92	15.72	0.67	0.015	0.758
WA-PLS	0.95	16.20	0.65	0.007	0.160

WA-PLS = weighted-averaging partial-least-squares method.

(Sadekov et al., 2016). However, the high numbers of *G. bulloides* observed throughout the studied interval of core SL163 suggest intense upwelling conditions and we therefore assume that we mainly sampled specimens of the cool-water genotype, type IIf, which is restricted to upwelling stations of the northern Oman margin (Sadekov et al., 2016).

4.3 Proxies of OMZ conditions and carbonate preservation

Trace-element distributions of manganese (Mn) and vanadium (V) were used as an indicator for bottom-water redox conditions and state of the OMZ, following Tribovillard et al. (2006). V is enriched throughout the studied interval and enrichment relative to average shale ranges from 1.0 to 1.7. With average values of 0.92, Mn is mostly depleted except for four short phases centred at 6.0, 6.3, 7.2 and 8.4 ka BP (Fig. 6g). The concentration of pteropod fragments ranges from 0 (pteropod barren) to 5.2×10^3 numbers per gram dry weight and PF fragmentation ranges between 0.1 and 12.2 % (Le and Shackleton, 1992).

5 Discussion

5.1 Interpretation of the two independent planktic foraminiferal SST proxies

A direct comparison of the Mg / Ca SST of *G. bulloides* and assemblage-based (consensus of IK and WA-PLS) summer SST reveals no linear relationship ($r = 0.02$, $p = 0.91$), although the binned time series show a weak positive linearity ($r = 0.24$, $p < 0.06$). This indicates that the low-frequency signals of both time series are linearly related. Furthermore, the time series of both proxy records reveal a common trend of increasing temperatures over the record (Fig. 6a–b) and are coherent on a wide range of frequencies. Significant (> 95 % confidence) coherence was found on ~ 1300-, ~ 110- and ~ 60-year periods, as well as on ~ 150-, ~ 90- and ~ 40-year periods (> 99 % confidence). Both SST records are thus in good general agreement, but Mg / Ca SSTs are on average 2.3 °C colder. This relative offset of the SST reconstructions might be attributed to timing differences during the recording of the respective proxy signal. *G. bulloides* is interpreted to carry the upwelling signal during peak production of this species (Peeters et al., 2002; Anand et al., 2008). Highest flux rates of *G. bulloides* are found from May to October, but with a clear maximum from late July to September (Curry et al., 1992; Conan and Brummer, 2000; Peeters et al., 2002). Furthermore, several stud-
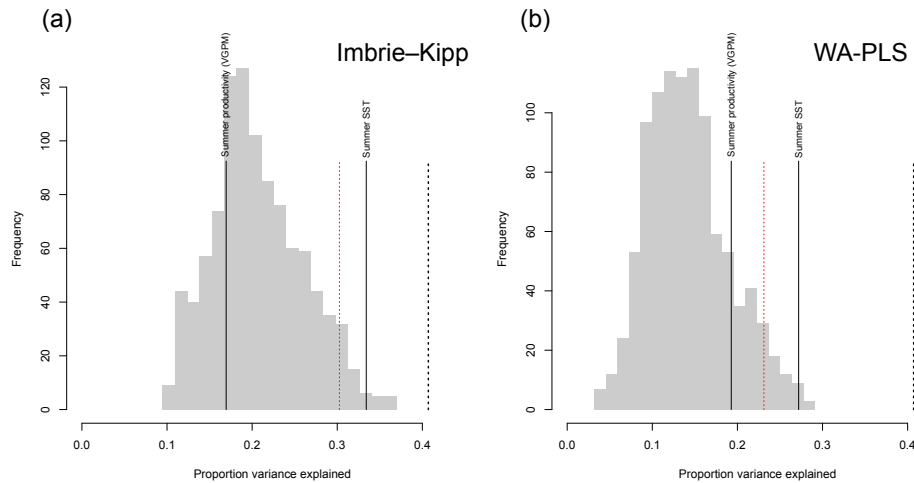
Figure 5. Results of the significance test of assemblage-based palaeoenvironmental reconstructions using the R package palaeoSig (Telford, 2015). The null distribution is produced by generating 999 random environmental variables and reconstructing these variables from PF assemblages of core SL163 using **(a)** the Imbrie–Kipp method (IK) and **(b)** the weighted-averaging partial-least-squares (WA-PLS) method. Grey shaded histograms indicate the amount of variance of the fossil data explained by the 999 random environmental variables, whereas the black vertical lines indicate the variance explained by the reconstruction of summer productivity (VGPM) and summer SST using the different methods. The red dashed line represents the 95th percentile of the null distribution; the black dashed line represents the variance explained by the first RDA axis. Thus, the proportion of variance explained by the IK method for the reconstruction of summer SST from the fossil dataset is higher than 95 % ($p = 0.015$) of reconstructions of 999 random environmental variables. The summer SST reconstruction from the WA-PLS method is higher than 99 % of the random reconstructions ($p = 0.007$). The VGPM-based reconstruction of summer surface primary productivity is not significant (IK: $p = 0.76$; WA-PLS: $p = 0.16$).

ies in the Arabian Sea (Peeters et al., 2002; Schiebel et al., 2004; Friedrich et al., 2012) and in the Java upwelling region (Mohtadi et al., 2011) indicate that *G. bulloides* thrives in coastal upwelling areas mostly within the mixed-layer and upper thermocline waters in the uppermost 50–60 m of the water column. Assemblage-based SST reconstructions are calibrated to the 10 m depth level of summer temperatures. We therefore interpret Mg / Ca values of *G. bulloides* to represent calcification temperatures of mixed-layer and upper thermocline waters during peak production of the late summer upwelling and assemblage-based SST reconstructions to represent a shallower SST average from July to September.

5.2 Evidence for early to mid-Holocene monsoon variability

The range of reconstructed water temperatures of 6.16 °C and a mean absolute deviation of 0.72 °C from Mg / Ca measurements of *G. bulloides* (upwelling SST) suggest that upwelling temperatures at the northern Oman margin fluctuated strongly and rapidly during the relatively short interval of the early to mid-Holocene covered by SL163. The amplitude of temperature fluctuations recorded by *G. bulloides* is approximately twice as high compared to oxygen isotope temperatures of the same species at the Somali margin during the early Holocene (Jung et al., 2002). Records from the Arabian Sea revealed that strongest ISM conditions occurred during the early Holocene around 8–11 ka BP (Staubwasser et al.,

2002; Gupta et al., 2003; Thamban et al., 2007), followed by a gradual weakening around 7 ka BP, which is concomitant with the time period of relatively warm assemblage-based SST (Fig. 7). However, the overall trend in our record is not consistent and instead indicates gradual weakening of ISM conditions established as early as 8 ka BP. Consistently low SSTs suggest that upwelling and ISM intensity was strongest during the intervals ∼ 7.5–8.1 ka, followed by events of strong ISM at ∼ 7.0–7.3 and 6.1 ka BP (Fig. 6a). Weaker ISM conditions are reflected by warmer-than-average SST values at 6, 6.5–6.9, 7.4 and 8.2 ka BP. Other palaeoceanographic records from the Arabian Sea (Fig. 7c–d) and stalagmite records from the nearby Hoti and Qunf caves (Fig. 6i–j) indicate low monsoonal precipitation at 6.3, 7.4 and 8.3 ka BP (Fleitmann et al., 2007; Neff et al., 2001), suggesting that summer monsoonal winds (reflected by low summer and upwelling SST) and amount of precipitation are in-phase during the early to mid-Holocene. This is an interesting finding, as Fleitmann et al. (2004) show an apparent decoupling of ISM precipitation amount and wind intensity (represented by percentage of *G. bulloides*) since the year ∼ 1900 AD, indicating that higher upwelling intensities do not necessarily involve increasing precipitation. Moreover, the most noticeable events of weak ISM conditions are in concordance with advection of North Atlantic drift ice from Bond et al. (2001) (Fig. 7e), centred at ∼ 5.9 (Bond event 4), ∼ 7.4 (Bond event 5) and ∼ 8.2 ka BP. The observation of a con-
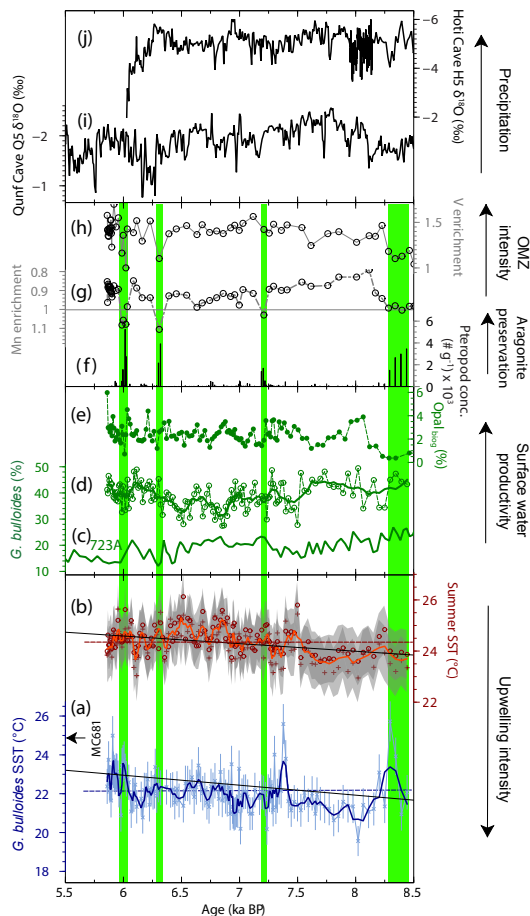
Figure 6. Time series of reconstructed SST from **(a)** the Mg / Ca ratio of *G. bulloides* (blue) indicating upwelling SST and **(b)** the consensus from the assemblage-based transfer function methods, IK and WA-PLS (red), indicating average summer SST (July–September). Thin lines and symbols represent real data; thick dashed lines represent the 3 pt running averages. Relative abundance of *G. bulloides* from IODP site 723A from Gupta et al. (2005) **(c)** and SL163 **(d)**, together with biogenic opal content **(e)**, indicate phases of increased surface water productivity. Aragonite preservation is indicated by the concentration of pteropod fragments **(f)** and bottom-water oxygen conditions, and state of the oxygen minimum zone (OMZ) is shown with relative enrichment or depletion of manganese **(g)** and vanadium **(h)**. Note the inverse relationship of both elements, as explained in the text. Stable oxygen isotopes of **(i)** Qunf Cave (Fleitmann et al., 2007) and **(j)** Hoti Cave stalagmites (Neff et al., 2001) expressing precipitation in Oman. Vertical solid green bars indicate periods of low biogenic opal content, concomitant with decreased OMZ intensity and increased aragonite preservation. Error bars for panel **(a)** were calculated by propagating the errors introduced by the Mg / Ca measurements and the Mg / Ca–temperature calibration (Gaussian error propagation; see Mohtadi et al. (2014)). Grey shading gives the uncertainty estimates for the transfer functions in panel **(b)**, based on the sample-specific root mean square error of prediction (RMSEP) using bootstrapping cross validation.
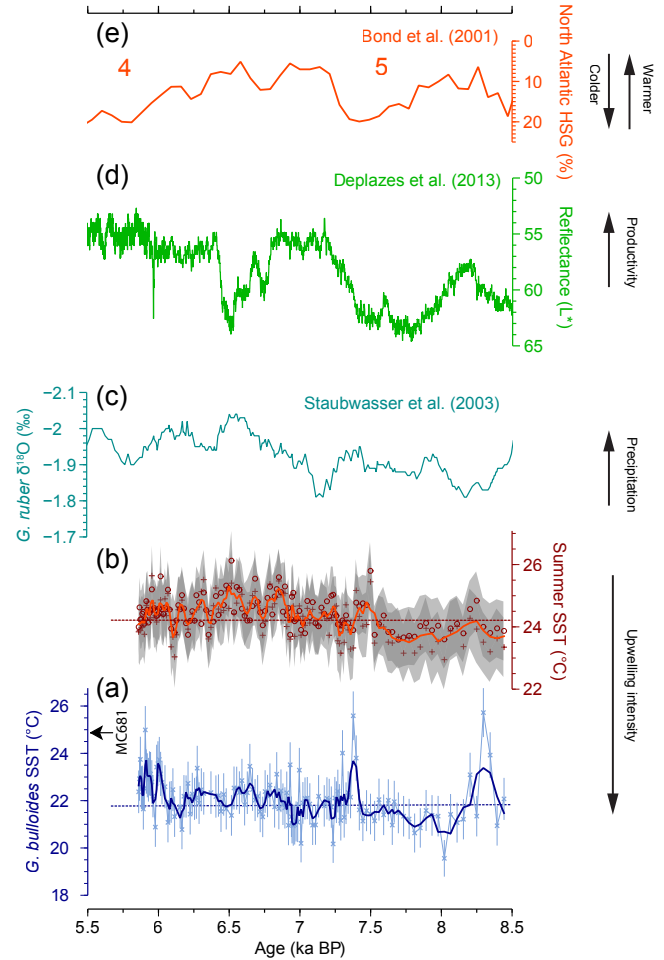
Figure 7. Comparison of SST time series from **(a)** the Mg / Ca ratio of *G. bulloides* and **(b)** assemblage-based transfer functions with **(c)** $\delta^{18}O$ ratio (‰) of *G. ruber* from core 63KA (Staubwasser et al., 2003) and **(d)** colour reflectance (L*) of core SO130-289KL (Deplazes et al., 2013) both from the Pakistan margin, indicative of precipitation **(c)** and productivity **(d)** associated with ISM intensity. **(e)** Hematite-stained grains (HSG, %) indicate ice rafting events and cold spells in the North Atlantic (Bond et al., 2001). Bond events 4 (~ 5.9 ka BP) and 5 (~ 7.4 ka BP) are indicated.

temporaneous occurrence of North Atlantic cold spells and weak Asian monsoon was previously found in speleothem (Dykoski et al., 2005; Fleitmann et al., 2007; Liu et al., 2013), lake (Menzel et al., 2014) and other marine records (Gupta et al., 2003). Thus, our findings are further evidence corroborating the presence of an atmospheric teleconnection linking North Atlantic climate to summer monsoonal conditions in tropical Asia during the early to mid-Holocene. However, in order to significantly assess millennial-scale cycles in the upwelling SST off the Oman margin, further studies are needed, as the time span of ~ 2.5 ka covered by our record is likely too short.
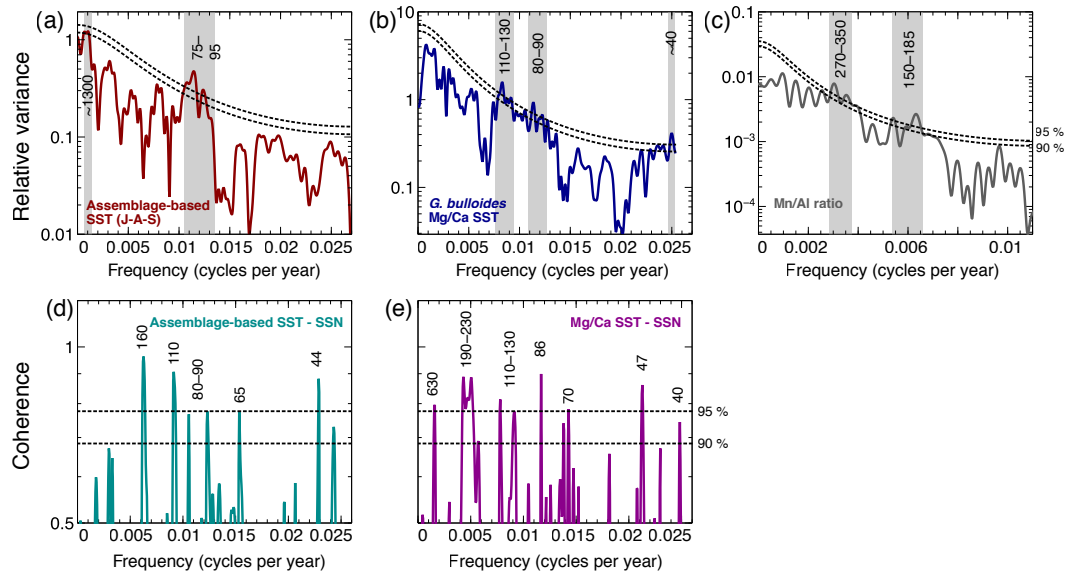
Figure 8. Results of the MTM spectral analysis show the frequency distribution and identified significant periodicities of the **(a)** assemblage-based SST record, **(b)** the SST record using Mg / Ca ratios of *G. bulloides* and **(c)** the Mn / Al ratio as a proxy for OMZ conditions. Black lines indicate 90 and 95 % significance levels against red noise. Cross-spectral coherence of both SST records **(d, e)** with the record of sunspot numbers (Solanki et al., 2004) indicates that both records significantly co-vary on a wide range of frequencies. All time series were trend-removed prior to the analyses.

MTM analysis revealed statistically significant periodicities of assemblage-based summer SST at ∼ 1300 and 75–95 years per cycle (Fig. 8a). Mg / Ca-based upwelling SSTs are modulated on frequencies at 110–130, 80–90 and ∼ 40 years (Fig. 8b). The longer ∼ 110–130-year cycle was previously found in a number of records from the Asian monsoon realm (Berger and von Rad, 2002; Dykoski et al., 2005; Gupta et al., 2005) and is close to the 132-year subharmonic of the Hale cycle (Attolini et al., 1990), previously identified to be modulating the Oman upwelling system during the Holocene (Gupta et al., 2005). The ∼ 80–90-year cycle has been observed in several studies of ISM variability (Neff et al., 2001; Fleitmann et al., 2003; Dykoski et al., 2005; Gupta et al., 2005) and was interpreted to be most likely influenced by the 88-year solar Gleissberg cycle. Turner et al. (2016) found, however, that periodicities within the range of the Gleissberg cycle are also common in random-walk simulations and could be statistical artefacts from the sampling resolution and the age model applied. In fact, the overall error of the reservoir correction of ±31 years is close to the observed periodicities, which might give an indication of why we found the Gleissberg cycle but not the longer-period (∼ 200–210 years) de Vries solar cycle. However, Duan et al. (2014) showed with a speleothem record from Dongge Cave (China), that coherency of eastern Asian monsoon precipitation and the solar Gleissberg cycle is persistent over the last 4 kyr, whereas coherency with the de Vries cycle was only observed over a short 1 kyr long period. Other Holocene

Asian monsoon records also showed periodicities similar to the Gleissberg cycle, while lacking the longer de Vries cycle (e.g. Wang et al., 1999; Sagawa et al., 2014). It could thus be hypothesised that the de Vries cycle is not detectable in our record, due to a transient link of the solar–monsoon relationship, potentially suppressed by changes in the ocean–atmosphere system in the El Niño–Southern Oscillation domain (Berkelhammer et al., 2010). We therefore tested a possible solar component on the decadal-scale forcing of our SST records by evaluating the coherence of both time series with the record of reconstructed sunspot numbers (Solanki et al., 2004). The coherence pattern reveals that both SST records and sunspot numbers are coherent on a wide range of periodicities (630, 190–230, 160, 110–130, 80–90, ∼ 70, ∼ 50 and ∼ 40 years per cycle; Fig. 8d and e). The Mg / Ca-based SST record shows the strongest coherency with cycles of the sunspot record in both the ∼ 88-year Gleissberg and the ∼ 190–230-year de Vries periodicities. This observation further strengthens the hypothesis that ISM variability is not only controlled by orbital-scale insolation forcing, indicated by the long-term trend of warming temperatures and decreasing ISM intensity, but also by solar forcing.

To illustrate the signature of the observed cycles in the data, band-pass-filter outputs of both SST records are shown in Fig. 9. Apparently, amplitude modulations of the filter outputs of both SST time series run largely synchronously. On the ∼ 132-year bandwidth, amplitude modulations of the Mg / Ca-based upwelling SST and total solar irradiance
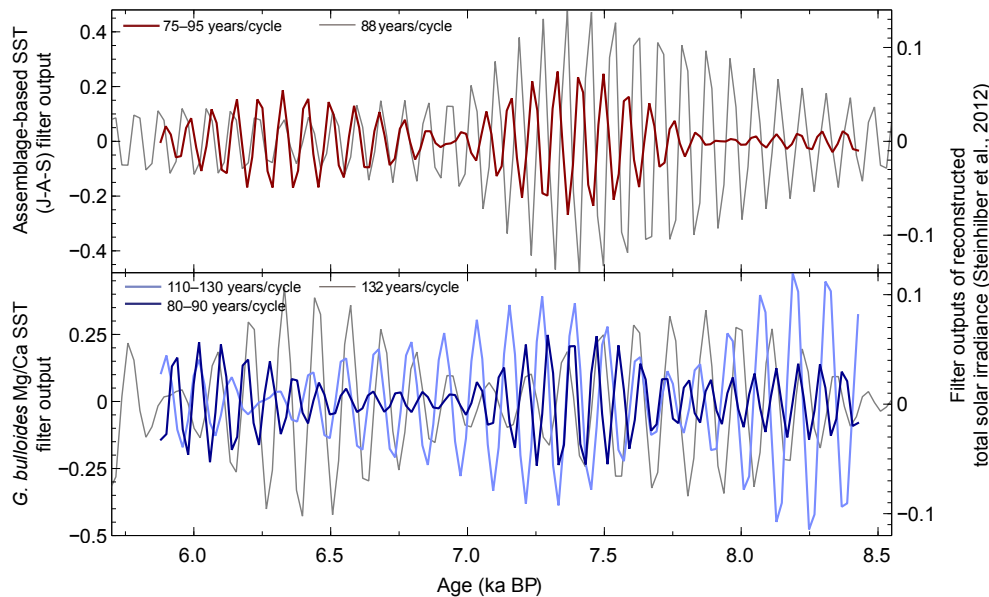
Figure 9. Comparison of filtered assemblage-based SST (red line, upper panel) and *G. bulloides* Mg / Ca SST (blue lines, lower panel) with filtered reconstructed total solar irradiance (TSI) from Steinhilber et al. (2012) (grey lines); 88 years per cycle are illustrated in the upper panel and 132 years per cycle in the lower panel. Filtered components were extracted using a Gaussian band-pass filter with a central frequency of 0.0118 cycles year^{-1} (~ 85-year cycle) and 0.0083 cycles year^{-1} (~ 120-year cycle), respectively, and a bandwidth of 0.001 cycles year^{-1} using the program AnalySeries 2.0.8 (Paillard et al., 1996).

(TSI) are offset by a lag of ~ 400 years. A direct forcing on this bandwidth seems unlikely, as modelling studies indicate a response of surface temperatures to solar forcing within less than 50 years (Seidenglanz et al., 2012). However, within the limits of our age model, comparison of the amplitude variations in the filter outputs from both SST time series and the TSI record of Steinhilber et al. (2012), filtered on the ~ 85-year Gleissberg bandwidth, apparently indicates synchrony of our SST records and TSI with maximum amplitude modulations of all three records centred at ~ 7.4 ka BP. Our new high-resolution record of summer and upwelling SST therefore provides further strong evidence that solar forcing persistently modulated ISM variability during the early to mid-Holocene after the summer insolation maximum, previously found from speleothem (Neff et al., 2001; Burns et al., 2002; Fleitmann et al., 2003; Dykoski et al., 2005; Wang et al., 2005; Duan et al., 2014) and marine records (von Rad et al., 1999; Wang et al., 1999; Gupta et al., 2005).

5.3 Carbonate preservation and bottom-water redox conditions

In order to study the interplay of ISM intensity and OMZ fluctuations, we compared our new multi-proxy reconstruction of summer SST to OMZ reconstructions of Böll (2014). This study previously evaluated ISM intensity and OMZ conditions during the deposition of SL163 in a spatial context using alkenone-derived annual mean SST, stable nitro-

gen isotopes and published OMZ reconstructions, concluding that changes in OMZ intensity were linked to variability in intermediate water ventilation and monsoon strength. Our new multi-proxy records that primarily respond to summer upwelling conditions enable the study of the interplay of ISM intensity and OMZ fluctuations during the early to mid-Holocene in more detail. Under oxic bottom-water conditions, Mn is precipitated as Mn oxyhydroxides. Under suboxic or hypoxic bottom-water conditions, MnO can be reduced to soluble Mn^{2+} and escape into the water column (Calvert and Pedersen, 1993; Calvert et al., 1996; Schnetger et al., 2000; Böning et al., 2004). Mn is mostly depleted in core SL163, indicating Mn loss through the OMZ, except for three short intervals of Mn enrichment centred at ~ 6.0, 6.3 and 7.2 ka BP, as well as from 8.3 ka BP to the end of the record (Fig. 6g). However, precipitation and fixation of Mn^{2+} in the sediment as $MnCO_3$ can occur when bottom waters become completely anoxic (Tribovillard et al., 2006; McKay et al., 2015). This finding corroborates the study of Böll (2014), who found increased denitrification, indicating more intense OMZ conditions during the intervals 5.9, 6.1, 6.4 and 7.2 ka BP (based on the same age model). V is precipitated under anoxic conditions (Emerson and Huested, 1991) and constant enrichment values between 1.0 and 1.7 relative to average shale also indicate permanent anoxic bottom-water conditions during the deposition of core SL163.

Carbonate preservation was assessed by PF fragmentation indices and the abundance of pteropod fragments in the sieve

fraction $> 150 \, \mu m$. Pteropod shells primarily consist of aragonite, the less stable polymorph of calcium carbonate as compared to calcite (Morse et al., 1980). In the northern Arabian Sea, aragonite has a modern compensation depth (ACD) of $\sim 500 \, m$ (W. H. Berger, 1978; Böning and Bard, 2009) and a lysocline at $\sim 1 \, km$ water depth (Böning and Bard, 2009), thus approximately 350 m below the station of core SL163. However, in high-productivity environments supra-lysoclinal dissolution can occur well above this depth, induced by respiration of organic matter and metabolic release of CO_2 (e.g. Milliman et al., 1999). Thus, enhanced pteropod preservation indicates either ACD deepening (Reichart et al., 2002) or less supra-lysoclinal dissolution due to decreased production of organic matter. Phases of increased concentrations of pteropod fragments are linked to the short intervals of slightly enriched Mn values (Fig. 6f–g). This indicates short phases of less corrosive bottom waters due to potentially weaker OMZ conditions. Furthermore, the variability in Mn / Al values (expressed as Mn enrichment) is modulated on dominant ~ 170- and ~ 310-year cycles (Fig. 8c), which are approximately one-half (170) and one-fourth (340) the ~ 80–90-year frequency of the Gleissberg cycle. This suggests that bottom-water oxygenation state is modulated on the same frequencies as SST variability and upwelling intensity.

The intervals of increased pteropod concentration and lower OMZ intensity at ~ 6, 6.3, 7.2 and 8.3–8.5 ka BP are linked to intervals of low biogenic opal and thus occurred when surface water productivity was diminished. The former three of these intervals also correspond to low abundances of the upwelling indicator species *G. bulloides* (Fig. 6d), but during the latter interval at 8.3–8.5 ka BP *G. bulloides* abundances are high ($> 45 \, \%$). In addition, Mg / Ca measurements of *G. bulloides* at 8.3 ka BP are $> 7 \, mmol \, mol^{-1}$ and inferred SSTs are $> 25.5 \, ^\circ C$. A similar feature of a very short warm excursion of Mg / Ca temperatures from *G. bulloides* with concomitantly high abundances of this species around 8 ka BP was observed by Anand et al. (2008) in their record from the Somali upwelling system. It may be speculated here whether a potential intrusion of the warm-water genotype of *G. bulloides* (Sadekov et al., 2016) during the short-lived period around 8.3 ka BP had occurred, leading to erroneously warm Mg / Ca temperature estimates during this period.

Regardless of the apparent difference in absolute temperatures, wavelet analysis and cross-wavelet transform (XWT) reveals three distinct intervals, two in the ~ 40–90-year band (6–6.2, 7.2–7.6 ka BP) and one in the ~ 110–130-year band (8.1–8.4 ka BP), where both records show significant common power (Fig. 10). The intervals correspond well with the phases of enhanced pteropod preservation and lower OMZ intensity. The cross-wavelet phase angle of XWT further indicates that both SST records are phase-shifted during these intervals. The arrows in Fig. 10 within the significant areas point mostly upwards, which indicates either that assemblage-based SSTs lead Mg / Ca SSTs by $\pi/2$, i.e. 90°, or that assemblage-based SSTs lag Mg / Ca SSTs by $3\pi/2$,
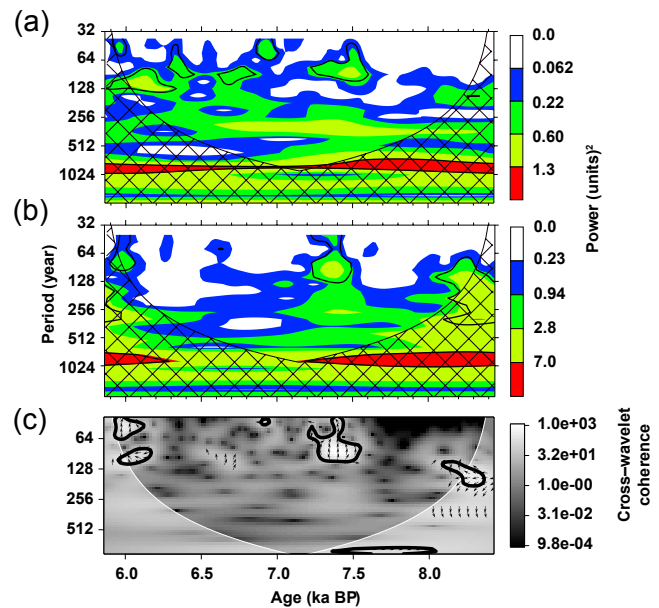

Figure 10. Continuous wavelet transform of **(a)** assemblage-based summer SST and **(b)** Mg / Ca-based upwelling SST. The 10 % significance level against red noise is shown as black contour lines. **(c)** Cross-wavelet transform (XWT) of the trend-removed Mg / Ca-based and assemblage-based SST time series. The 5 % significance level is shown as thick contours. Relative phasing of both records is indicated by arrows. Arrows within the significant intervals point mostly upwards, which indicates a consistent phase shift of both records by 90 or 270°, respectively, of assemblage-based SST relative to Mg / Ca-based SST. The cone of influence, where edge artefacts might be introduced, is indicated by hatching and white shading, respectively.

i.e. 270°. Although these phases are relatively short-lived and both scenarios seem reasonable from the visual comparison of the two SST time series, a systematic lead of faunal SST reconstructions compared to alkenone-derived SST was previously found by Cayre and Bard (1999) in a study from the eastern Arabian Sea. However, their study observed a delay of several thousands of years, which was potentially produced by strong productivity changes (Bard, 2001). It should be noted that the phase relationships at the longer wavelength could be erroneous, as the behaviour is not consistent and partly truncated by edge effects below the cone of influence.

Several studies in the Arabian Sea indicate an alternating influence of different water masses during the deglacial and early Holocene (Zahn and Pedersen, 1991; Jung et al., 2001; Schmiedl and Leuschner, 2005; Gupta et al., 2008; Jung et al., 2009). The site of core SL163 is within the modern range of intermediate water masses, which form a mixture of RSW, PGW and IOCW down to $\sim 1500 \, m$ water depth (Emery and Meincke, 1986; Shetye et al., 1994). During the last glacial stage, the outflow from the two mediterranean basins connected to the Arabian Sea (Red Sea and Persian

Gulf) was highly suppressed due to lowering of the global sea level potentially close to or even below the respective sill depths (Rohling and Zachariasse, 1996). Gupta et al. (2008) discussed the finding that ventilation changes at the northern Oman margin during the early Holocene are distant to RSW and are more likely attributed to an alternating contribution of North Atlantic Deep Water to the deeper water masses. In comparison to their study site, our core site is further north, close to the modern Ras Al Hadd frontal zone, where PGW enters the Arabian Sea. At the station of SL163, modern PGW reaches down to 400 m (Fig. 1). During phases of more restricted water exchange and increased evaporation, subsurface salinities in the Persian Gulf might have been higher, which could have enabled PGW to reach the core site at deeper depth. However, the modern oxygen input of PGW is very low and OMZ conditions at this depth are still fully hypoxic. Instead, the concomitant occurrence of high common cross-wavelet power of the SST records (Fig. 10) with less corrosive bottom waters indicates that deep-water conditions are linked to SST variations and atmospheric forcing was intimately linked to the deep-water properties.

6 Conclusions

Among the environmental variables investigated, summer SST primarily controls the underlying variability in PF assemblages from the northwestern Arabian Sea. Statistically significant reconstructions of summer SST from PF assemblages and Mg / Ca SST from *G. bulloides* are colder than present summer temperatures, indicating vigorous monsoonal winds and upwelling intensity during the early to mid-Holocene. ISM conditions were generally strongest around 8 ka BP and gradually decreased towards 5.8 ka BP. The trend of weakening monsoon conditions was interrupted by decadal-scale episodes of intensified ISM around ~ 7 and 6.2 ka BP, which is concomitant with pluvial episodes indicated by the Oman speleothem records. Summer SST fluctuations furthermore reveal that upwelling intensity was coupled to decadal-to-centennial-scale sunspot cycles.

Low monsoonal conditions, indicated by warm upwelling SST and summer SST and low surface water productivity, are associated with enhanced pteropod preservation and weaker OMZ conditions. Enrichment of manganese as a proxy for bottom-water oxygenation varies on multiples of the dominant ~ 80–90-year Gleissberg cycle, suggesting that upwelling intensity and OMZ conditions are modulated by solar activity. We therefore conclude that, instead of intermediate water mass changes, atmospheric forcing is the main driver of OMZ conditions.

References

Anand, P., Kroon, D., Singh, A. D., and Ganssen, G.: Coupled sea surface temperature-seawater δ^{18}O reconstructions in the Arabian Sea at the millennial scale for the last 35 ka, Paleoceanography, 23, PA4207, doi:10.1029/2007PA001564, 2008.

Anderson, D. M., Overpeck, J. T., and Gupta, A. K.: Increase in the Asian Southwest Monsoon During the Past Four Centuries, Science, 297, 596–599, 2002.

Attolini, M. R., Cecchini, S., Galli, M., and Nanni, T.: On the persistence of the 22 y solar cycle, Sol. Phys., 125, 389–398, 1990.

Bard, E.: Comparison of alkenone estimates with other paleotemperature proxies, Geochem. Geophy. Geosy., 2, 1002, doi:10.1029/2000GC000050, 2001.

Barker, S., Greaves, M., and Elderfield, H.: A study of cleaning procedures used for foraminiferal Mg / Ca paleothermometry, Geochem. Geophys. Geosy., 4, 8407, doi:10.1029/2003GC000559, 2003.

Bé, A.: Foraminifera families: *Globigerinidae* and *Globorotalidae*, in: Fiches d'Identification du Zooplankton. Sheet 108, edited by: Fraser, J. H., 1–8, Conseil Perm. Internat. Explor. Mer, Charlottenlund, Denmark, 1967.

Bé, A. and Hutson, W. H.: Ecology of planktonic foraminifera and biogeographic patterns of life and fossil assemblages in the Indian Ocean, Micropaleontology, 23, 369–414, doi:10.2307/1485406, 1977.

Berger, A. L.: Long-term variations of daily insolation and Quaternary climatic changes, J. Atmos. Sci., 35, 2362–2367, 1978.

Berger, W. H.: Deep-sea carbonate: Pteropod distribution and the aragonite compensation depth, Deep-Sea Res., 25, 447–452, 1978.

Berger, W. H. and von Rad, U.: Decadal to millennial cyclicity in varves and turbidites from the Arabian Sea: hypothesis of tidal origin, Global Planet. Change, 34, 313–325, 2002.

Berkelhammer, M., Sinha, A., Mudelsee, M., Cheng, H., Edwards, R. L., and Cannariato, K.: Persistent multidecadal power of the Indian Summer Monsoon, Earth Planet. Sc. Lett., 290, 166–172, doi:10.1016/j.epsl.2009.12.017, 2010.

Birks, H.: Numerical tools in palaeolimnology–Progress, potentialities, and problems, J. Paleolimnol., 20, 307–322, 1998.

Blaauw, M.: Methods and code for 'classical' age-modelling of radiocarbon sequences, Quaternary Geochronol., 5, 512–518, 2010.

Bohrmann, G., Lahajnar, N., Gaye, B., Spiess, V., and Betzler, C.: Nitrogen Cycle, Cold Seeps, Carbonate Platform Development in the Northwestern Indian Ocean, Cruise No.74, 31 August–22 December 2007, University of Hamburg, 2010.

Böll, A.: Reconstruction of the Holocene monsoon climate variability in the Arabian Sea based on alkenone sea surface temperature, primary productivity and denitrification proxies, Ph.D. thesis, University of Hamburg, 2014.

Bond, G., Kromer, B., Beer, J., Muscheler, R., Evans, M. N., Showers, W., Hoffmann, S., Lotti-Bond, R., Hajdas, I., and Bonani, G.: Persistent solar influence on North Atlantic climate during the Holocene., Science, 294, 2130–2136, 2001.

Böning, P. and Bard, E.: Millennial/centennial-scale thermocline ventilation changes in the Indian Ocean as reflected by aragonite preservation and geochemical variations in Arabian Sea sediments, Geochim. Cosmochim. Ac., 73, 6771–6788, 2009.

Böning, P., Brumsack, H. J., and Böttcher, M. E.: Geochemistry of Peruvian near-surface sediments, Geochim. Cosmochim. Ac., 68, 4429–4451, 2004.

Brown, S. J. and Elderfield, H.: Variations in Mg / Ca and Sr/Ca ratios of planktonic foraminifera caused by postdepositional dissolution: Evidence of shallow Mg-dependent dissolution, Paleoceanography, 11, 543–551, 1996.

Burns, S. J., Fleitmann, D., Mudelsee, M., Neff, U., Matter, A., and Mangini, A.: A 780-year annually resolved record of Indian Ocean monsoon precipitation from a speleothem from south Oman, J. Geophys. Res., 107, 4434, doi:10.1029/2001JD001281, 2002.

Calvert, S. E. and Pedersen, T. F.: Geochemistry of Recent oxic and anoxic marine sediments: Implications for the geological record, Mar. Geol., 113, 67–88, 1993.

Calvert, S. E., Bustin, R. M., and Ingall, E. D.: Influence of water column anoxia and sediment supply on the burial and preservation of organic carbon in marine shales, Geochim. Cosmochim. Ac., 60, 1577–1593, 1996.

Cayre, O. and Bard, E.: Planktonic foraminiferal and alkenone records of the last deglaciation from the Eastern Arabian Sea, Quaternary Res., 52, 337–342, 1999.

Clemens, S., Prell, W., Murray, D., Shimmield, G., and Weedon, G.: Forcing Mechanisms of the Indian-Ocean Monsoon, Nature, 353, 720–725, 1991.

Conan, S. and Brummer, G.: Fluxes of planktic foraminifera in response to monsoonal upwelling on the Somalia Basin margin, Deep-Sea Res. Pt. II, 47, 2207–2227, 2000.

Conan, S. M. H., Ivanova, E. M., and Brummer, G. J. A.: Quantifying carbonate dissolution and calibration of foraminiferal dissolution indices in the Somali Basin, Mar. Geol., 182, 325–349, 2002.

Conkright, M. E., Levitus, S., OBrien, T., Boyer, T. P., Stephens, C., Johnosn, D., Stathoplos, L., Baranova, O., Antonov, J., Gelfeld, R., Burney, J., Rochester, J., and Forgy, C.: World Ocean Database 1998 Documentation and Quality Control, Silver SPring, MD, 1998.

Conley, D. J.: An interlaboratory comparison for the measurement of biogenic silica in sediments, Mar. Chem., 63, 39–48, 1998.

Courtney, M. and Gordon, M.: Determining the number of factors to retain in EFA: Using the SPSS R-Menu v2. 0 to make more judicious estimations, Practical Assessment, 18, 2013.

Curry, W. B., Ostermann, D. R., Guptha, M. V. S., and Ittekkot, V.: Foraminiferal production and monsoonal upwelling in the Arabian Sea: evidence from sediment traps, in: Upwelling Systems Evolution Since the Early Miocene, edited by: Summerhayes, C. P., Prell, W. L., and Emeis, K. C., 93–106, London, 1992.

Dahl, K. A. and Oppo, D. W.: Sea surface temperature pattern reconstructions in the Arabian Sea, Paleoceanography, 21, PA1014, doi:10.1029/2005PA001162, 2006.

Dekens, P. S., Lea, D. W., Pak, D. K., and Spero, H. J.: Core top calibration of Mg / Ca in tropical foraminifera: Refining paleotemperature estimation, Geochem. Geophy. Geosy., 3, 1–29, 2002.

DeMaster, D. J.: The supply and accumulation of silica in the marine environment, Geochim. Cosmochim. Ac., 45, 1715–1732, 1981.

Deplazes, G., Lückge, A., Peterson, L. C., Timmermann, A., Hamann, Y., Hughen, K. A., Röhl, U., Laj, C., Cane, M. A., Sigman, D. M., and Haug, G. H.: Links between tropical rainfall and North Atlantic climate during the last glacial period, Nat, Geosci., 6, 213–217, doi:10.1038/ngeo1712, 2013.

Duan, F., Wang, Y., Shen, C.-C., Wang, Y., Cheng, H., Wu, C.-C., Hu, H.-M., Kong, X., Liu, D., and Zhao, K.: Evidence for solar cycles in a late Holocene speleothem record from Dongge Cave, China., Scientific Reports, 4, 5159, doi:10.1038/srep05159, 2014.

Dykoski, C. A., Edwards, R. L., Cheng, H., Yuan, D., Cai, Y., Zhang, M., Lin, Y., Qing, J., An, Z., and Revenaugh, J.: A high-resolution, absolute-dated Holocene and deglacial Asian monsoon record from Dongge Cave, China, Earth Planet. Sc. Lett., 233, 71–86, 2005.

Elderfield, H. and Ganssen, G.: Past temperature and delta18O of surface ocean waters inferred from foraminiferal Mg / Ca ratios, Nature, 405, 442–445, 2000.

Emeis, K.-C., Anderson, D. M., Kroon, D., and Schulz-Bull, D.: Sea-surface temperatures and history of monsoon upwelling in the Northeastern Arabian Sea during the last 500,000 years, Quaternary Res., 43, 355–361, 1995.

Emerson, S. R. and Huested, S. S.: Ocean anoxia and the concentrations of molybdenum and vanadium in seawater, Mar. Chem., 34, 177–196, 1991.

Emery, W. J. and Meincke, J.: Global Water Masses – Summary and Review, Oceanol. Acta, 9, 383–391, 1986.

Fairbanks, R. G., Sverdlove, M., Free, R., Wiebe, P. H., and Bé, A.: Vertical-Distribution and Isotopic Fractionation of Living Planktonic-Foraminifera From the Panama Basin, Nature, 298, 841–844, 1982.

Farías, L., Fernández, C., Faúndez, J., Cornejo, M., and Alcaman, M. E.: Chemolithoautotrophic production mediating the cycling of the greenhouse gases N_2O and CH_4 in an upwelling ecosystem, Biogeosciences, 6, 3053–3069, doi:10.5194/bg-6-3053-2009, 2009.

Findlater, J.: A major low-level air current near the Indian Ocean during the northern summer, Q. J. Roy. Meteor. Soc., 95, 362–380, 1969.

Fleitmann, D., Burns, S. J., Mudelsee, M., Neff, U., Kramers, J., Mangini, A., and Matter, A.: Holocene forcing of the Indian

monsoon recorded in a stalagmite from Southern Oman, Science, 300, 1737–1739, 2003.

Fleitmann, D., Burns, S. J., Neff, U., Mudelsee, M., Mangini, A., and Matter, A.: Palaeoclimatic interpretation of high-resolution oxygen isotope profiles derived from annually laminated speleothems from Southern Oman, Quaternary Sci. Rev., 23, 935–945, 2004.

Fleitmann, D., Burns, S. J., Mangini, A., and Mudelsee, M.: Holocene ITCZ and Indian monsoon dynamics recorded in stalagmites from Oman and Yemen (Socotra), Quaternary Sci. Rev., 26, 170–188, 2007.

Fontugne, M., Carre, M., Bentaleb, I., Julien, M., and Lavallee, D.: Radiocarbon reservoir age variations in the south Peruvian upwelling during the Holocene, Radiocarbon, 46, 531–537, 2004.

Friedrich, O., Schiebel, R., Wilson, P. A., and Weldeab, S.: Influence of test size, water depth, and ecology on Mg / Ca, Sr/Ca, δ 18 O and δ 13 C in nine modern species of planktic foraminifers, Earth Planet Sc. Lett., 319–320, 133–145, 2012.

Ganssen, G. M., Peeters, F. J. C., Metcalfe, B., Anand, P., Jung, S. J. A., Kroon, D., and Brummer, G.-J. A.: Quantifying sea surface temperature ranges of the Arabian Sea for the past 20 000 years, Clim. Past, 7, 1337–1349, doi:10.5194/cp-7-1337-2011, 2011.

Garcia, H. E., Locarini, R. A., Boyer, T. P., and Antonov, J. I.: World Ocean Atlas 2009, Volume 3: Dissolved Oxygen, Apparent Oxygen Utilization and Oxygen Saturation, in: A. Mishonov Technical Ed., edited by: Levitus, S., p. 40, U.S. Government Printing Office, Washington D.C., 2010.

Ghil, M., Allen, M. R., Dettinger, M. D., Ide, K., Kondrashov, D., Mann, M. E., Robertson, A. W., Saunders, A., Tian, Y., Varadi, F., and Yiou, P.: Advanced spectral methods for climatic time series, Rev. Geophys., 40, 1–41, 2002.

Godad, S. P., Naidu, P. D., and Malmgren, B. A.: Sea surface temperature changes during May and August in the western Arabian Sea over the last 22kyr: Implications as to shifting of the upwelling season, Mar. Micropaleontol., 78, 25–29, 2011.

Greaves, M., Caillon, N., Rebaubier, H., Bartoli, G., Bohaty, S., Cacho, I., Clarke, L., Cooper, M., Daunt, C., Delaney, M., deMenocal, P., Dutton, A., Eggins, S., Elderfield, H., Garbe-Schoenberg, D., Goddard, E., Green, D., Groeneveld, J., Hastings, D., Hathorne, E., Kimoto, K., Klinkhammer, G., Labeyrie, L., Lea, D. W., Marchitto, T., Martínez-Botí, M. A., Mortyn, P. G., Ni, Y., Nuernberg, D., Paradis, G., Pena, L., Quinn, T., Rosenthal, Y., Russell, A., Sagawa, T., Sosdian, S., Stott, L., Tachikawa, K., Tappa, E., Thunell, R., and Wilson, P. A.: Interlaboratory comparison study of calibration standards for foraminiferal Mg / Ca thermometry, Geochem. Geophy. Geosy., 9, Q08010, doi:10.1029/2008GC001974, 2008.

Grinsted, A., Moore, J. C., and Jevrejeva, S.: Application of the cross wavelet transform and wavelet coherence to geophysical time series, Nonlin. Processes Geophys., 11, 561–566, doi:10.5194/npg-11-561-2004, 2004.

Gupta, A. K., Anderson, D. M., and Overpeck, J. T.: Abrupt changes in the Asian southwest monsoon during the Holocene and their links to the North Atlantic Ocean, Nature, 421, 354–357, 2003.

Gupta, A. K., Das, M., and Anderson, D. M.: Solar influence on the Indian summer monsoon during the Holocene, Geophys. Res. Lett., 32, L17703, doi:10.1029/2005GL022685, 2005.

Gupta, A. K., Clemens, S. C., Das, M., and Mukherjee, B.: Benthic foraminiferal faunal and isotopic changes as recorded in Holocene sediments of the northwest Indian Ocean, Paleoceanography, 23, PA2214, doi:10.1029/2007PA001546, 2008.

Hemleben, C., Spindler, M., and Anderson, O. R.: Modern planktonic foraminifera, Springer Berlin Heidelberg, 1989.

Horn, J. L.: A rationale and test for the number of factors in factor analysis, Psychometrika, 30, 179–185, 1965.

Huguet, C., Kim, J.-H., Sinninghe Damsté, J. S., and Schouten, S.: Reconstruction of sea surface temperature variations in the Arabian Sea over the last 23 kyr using organic proxies (TEX 86and U 37K'), Paleoceanography, 21, doi:10.1029/2005PA001215, 2006.

Hutson, W. H. and Prell, W. L.: A paleoecological transfer function, FI-2, for Indian Ocean planktonic foraminifera, J. Paleontol., 54, 381–399, 1980.

Imbrie, J. and Kipp, N. G. A.: New micropaleontologic method for quantitative paleoclimatology: application to Late Pleistocene Carribean core, in: The Late Cenozoic Glacial Ages, edited by: Turekian, K. K., 71–182, New Haven, Conn., 1971.

Juggins, S.: rioja: Analysis of Quaternary Science Data, R package version (0.8–7), 2015.

Jung, S., Kroon, D., Ganssen, G., and Peeters, F.: Enhanced Arabian Sea intermediate water flow during glacial North Atlantic cold phases, Earth Planet. Sc. Lett., 280, 220–228, 2009.

Jung, S. J. A., Ganssen, G. M., and Davies, G. R.: Multidecadal variations in the Early Holocene outflow of Red Sea water into the Arabian Sea, Paleoceanography, 16, 658–668, 2001.

Jung, S. J. A., Davies, G. R., Ganssen, G., and Kroon, D.: Decadal-centennial scale monsoon variations in the Arabian Sea during the Early Holocene, Geochem. Geophy. Geosy., 3, 1–10, 2002.

Kennett, D. J. and Kennett, J. P.: Influence of Holocene marine transgression and climate change on cultural evolution in southern Mesopotamia, in: Climate Change and Cultural Dynamics A Global Perspective on Mid-Holocene Transitions, edited by: Anderson, D. G., Maasch, K. A., and Sandweiss, D. H., Climate change and . . . , 2007.

Kucera, M., Weinelt, M., Kiefer, T., Pflaumann, U., Hayes, A., Weinelt, M., Chen, M.-T., Mix, A. C., Barrows, T. T., Cortijo, E., Duprat, J., Juggins, S., and Waelbroeck, C.: Reconstruction of sea-surface temperatures from assemblages of planktonic foraminifera: multi-technique approach based on geographically constrained calibration data sets and its application to glacial Atlantic and Pacific Oceans, Quaternary Sci. Rev., 24, 951–998, 2005.

Kuper, R. and Kröpelin, S.: Climate-Controlled Holocene Occupation in the Sahara: Motor of Africa's Evolution, Science, 313, 803–807, 2006.

Kutzbach, J. E. and Street-Perrott, F. A.: Milankovitch forcing of fluctuations in the level of tropical lakes from 18 to 0 kyr BP, Nature, 317, 130–134, 1985.

Le, J. and Shackleton, N. J.: Carbonate dissolution fluctuations in the western Equatorial Pacific during the late Quaternary, Paleoceanography, 7, 21–42, 1992.

Liu, Y.-H., Henderson, G. M., Hu, C.-Y., Mason, A. J., Charnley, N., Johnson, K. R., and Xie, S.-C.: Links between the East Asian monsoon and North Atlantic climate during the 8,200 year event, Nat. Geosci., 6, 117–120, 2013.

Locarnini, R. A., Mishonov, A. V., Antonov, J. I., Boyer, T. P., and Garcia, H. E.: World Ocean Atlas 2009, Volume 1: Temperature,

in: A. Mishonov Technical Ed., edited by: Levitus, S., p. 40, U.S. Government Printing Office, Washington D.C., 2010.

Madhupratap, M., Prasanna Kumar, S., Bhattathiri, P. M. A., Dileep Kumar, M., Raghukumar, S., Nair, K. K. C., and Ramaiah, N.: Mechanism of the biological response to winter cooling in the northeastern Arabian Sea, Nature, 384, 549–552, 1996.

Mann, M. E. and Lees, J. M.: Robust estimation of background noise and signal detection in climatic time series, Climatic Change, 33, 409–445, 1996.

McKay, C. L., Groeneveld, J., Filipsson, H. L., Gallego-Torres, D., Whitehouse, M. J., Toyofuku, T., and Romero, O. E.: A comparison of benthic foraminiferal Mn / Ca and sedimentary Mn / Al as proxies of relative bottom-water oxygenation in the low-latitude NE Atlantic upwelling system, Biogeosciences, 12, 5415–5428, doi:10.5194/bg-12-5415-2015, 2015.

Menzel, P., Gaye, B., Mishra, P. K., Anoop, A., Basavaiah, N., Marwan, N., Plessen, B., Prasad, S., Riedel, N., Stebich, M., and Wiesner, M. G.: Linking Holocene drying trends from Lonar Lake in monsoonal central India to North Atlantic cooling events, Palaeogeogr. Palaeoclimatol. Palaeoecol., 410, 164–178, doi:10.1016/j.palaeo.2014.05.044, 2014.

Milliman, J. D., Troy, P. J., Balch, W. M., and Adams, A. K.: Biologically mediated dissolution of calcium carbonate above the chemical lysocline?, Deep-Sea Res. Pt. I, 46, 1653–1669, 1999.

Mohan, R., Verma, K., Mergulhao, L. P., Sinha, D. K., Shanvas, S., and Guptha, M. V. S.: Seasonal variation of pteropods from the Western Arabian Sea sediment trap, Geo-Mar. Lett., 26, 265–273, 2006.

Mohtadi, M., Oppo, D. W., Lückge, A., DePol-Holz, R., Steinke, S., Groeneveld, J., Hemme, N., and Hebbeln, D.: Reconstructing the thermal structure of the upper ocean: Insights from planktic foraminifera shell chemistry and alkenones in modern sediments of the tropical eastern Indian Ocean, Paleoceanography, 26, PA3219, doi:10.1029/2011PA002132, 2011.

Mohtadi, M., Prange, M., Oppo, D. W., De Pol-Holz, R., Merkel, U., Zhang, X., Steinke, S., and Lückge, A.: North Atlantic forcing of tropical Indian Ocean climate, Nature, 509, 76–80, 2014.

Morse, J. W., Mucci, A., and Millero, F. J.: The solubility of calcite and aragonite in seawater at various salinities, temperatures and atmosphere total pressure, Geochim. Cosmochim. Ac., 44, 85–94, 1980.

Munz, P. M., Siccha, M., Lückge, A., Böll, A., Kucera, M., and Schulz, H.: Decadal-resolution record of winter monsoon intensity over the last two millennia from planktic foraminiferal assemblages in the northeastern Arabian Sea, The Holocene, 25, 1756–1771, 2015.

Munz, P. M., Lückge, A., Siccha, M., Böll, A., Forke, S., Kucera, M., and Schulz, H.: The Indian winter monsoon and its response to external forcing over the last two and a half centuries, Clim. Dynam., 1–12, doi:10.1007/s00382-016-3403-1, 2016.

Munz, P., Steinke, S., Böll, A., Lückge, A., Groeneveld, J., Kucera, M., and Schulz, H.: Decadal resolution record of sediment core M74/1b_944-6 (SL 163), doi:10.1594/PANGAEA.874696, Supplement to: Munz, P. et al. (2016): Decadal resolution record of Oman margin upwelling indicates persistent solar forcing of the Indian summer monsoon after the early Holocene summer insolation maximum, Climate of the Past Discussions, 1–31, doi:10.5194/cp-2016-107, 2017.

Murtugudde, R., Seager, R., and Thoppil, P.: Arabian Sea response to monsoon variations, Paleoceanography, 22, PA4217, doi:10.1029/2007PA001467, 2007.

Naidu, P. D. and Malmgren, B. A.: A High-resolution record of Late Quaternary upwelling along the Oman Margin, Arabian Sea based on planktonic foraminifera, Paleoceanography, 11, 129–140, 1996.

Neff, U., Burns, S. J., Mangini, A., Mudelsee, M., Fleitmann, D., and Matter, A.: Strong coherence between solar variability and the monsoon in Oman between 9 and 6 kyr ago, Nature, 411, 290–293, 2001.

Oksanen, J., Blanchet, F. G., Kindt, R., Legendre, P., Minchin, P. R., O'Hara, R. B., Simpson, G. L., Solymos, P., Stevens, M. H. H., and Wagner, H.: vegan: Community Ecology Package, r package version 2.3-1 edn., 2015.

Paillard, D., Labeyrie, L., and Yiou, P.: Macintosh program performs time-series analysis, Eos Trans. AGU, 77, 379, doi:10.1029/96EO00259, 1996.

Paulmier, A., Ruiz-Pino, D., and Garçon, V.: CO_2 maximum in the oxygen minimum zone (OMZ), Biogeosciences, 8, 239–252, doi:10.5194/bg-8-239-2011, 2011.

Peeters, F. J. C. and Brummer, G. J. A.: The seasonal and vertical distribution of living planktic foraminifera in the NW Arabian Sea, Geological Society, London, Special Publications, 195, 463–497, 2002.

Peeters, F. J. C., Brummer, G.-J. A., and Ganssen, G.: The effect of upwelling on the distribution and stable isotope composition of *Globigerina bulloides* and *Globigerinoides ruber* (planktic foraminifera) in modern surface waters of the NW Arabian Sea, Global Planet. Change, 34, 269–291, 2002.

Pflaumann, U., Duprat, J., Pujol, C., and Labeyrie, L.: SIMMAX: A modern analog technique to deduce Atlantic sea surface temperatures from planktonic foraminifera in deep-sea sediments, Paleoceanography, 11, 15–35, 1996.

Prasanna Kumar, S. and Prasad, T. G.: Formation and spreading of Arabian Sea high-salinity water mass, J. Geophys. Res., 104, 1455–1464, 1999.

Prell, W. L. and Curry, W. B.: Faunal and isotopic indices of monsoonal upwelling-western arabian sea, Oceanol. Acta, 4, 91–98, 1981.

R Core Team: R: A Language and Environment for Statistical Computing, R Foundation for Statistical Computing, Vienna, Austria, 2015.

Reichart, G.-J., Schenau, S. J., De Lange, G. J., and Zachariasse, W. J.: Synchroneity of oxygen minimum zone intensity on the Oman and Pakistan Margins at sub-Milankovitch time scales, Mar. Geol., 185, 403–415, 2002.

Reimer, P. J., Bard, E., Bayliss, A., Beck, J. W., Blackwell, P. G., Bronk Ramsey, C., Buck, C. E., Cheng, H., Edwards, R. L., Friedrich, M., Grootes, P. M., Guilderson, T. P., Haflidason, H., Hajdas, I., Hatté, C., Heaton, T. J., Hoffmann, D. L., Hogg, A. G., Hughen, K. A., Kaiser, K. F., Kromer, B., Manning, S. W., Niu, M., Reimer, R. W., Richards, D. A., Scott, E. M., Southon, J. R., Staff, R. A., Turney, C. S. M., and van der Plicht, J.: IntCal13 and Marine13 radiocarbon age calibration curves 0–50,000 years cal BP, Radiocarbon, 55, 1869–1887, 2013.

Rohling, E. J. and Zachariasse, W. J.: Red Sea outflow during the last glacial maximum, Quaternary Int., 31, 77–83, 1996.

Sadekov, A. Y., Darling, K. F., Ishimura, T., Wade, C. M., Kimoto, K., Singh, A. D., Anand, P., Kroon, D., Jung, S., Ganssen, G., Ganeshram, R., Tsunogai, U., and Elderfield, H.: Geochemical imprints of genotypic variants of Globigerina bulloides in the Arabian Sea, Paleoceanography, 31, 2016PA002947, doi:10.1002/2016PA002947, 2016.

Sagawa, T., Kuwae, M., Tsuruoka, K., Nakamura, Y., Ikehara, M., and Murayama, M.: Solar forcing of centennial-scale East Asian winter monsoon variability in the mid- to late Holocene, Earth Planet. Sc. Lett., 395, 124–135, 2014.

Schiebel, R., Zeltner, A., Treppke, U. F., and Waniek, J. J.: Distribution of diatoms, coccolithophores and planktic foraminifers along a trophic gradient during SW monsoon in the Arabian Sea, Mar. Micropaleontol., 51, 345–371, 2004.

Schlitzer, R.: Ocean Data View, http://odv.awi.de, 2015.

Schmiedl, G. and Leuschner, D. C.: Oxygenation changes in the deep western Arabian Sea during the last 190,000 years: Productivity versus deepwater circulation, Paleoceanography, 20, PA2008, doi:10.1029/2004PA001044, 2005.

Schnetger, B., Brumsack, H. J., Schale, H., and Hinrichs, J.: Geochemical characteristics of deep-sea sediments from the Arabian Sea: a high-resolution study, Deep-Sea Res., 47, 2735–2768, 2000.

Schulz, H., von Rad, U., and Ittekkot, V.: Planktic foraminifera, particle flux and oceanic productivity off Pakistan, NE Arabian Sea: modern analogues and application to the palaeoclimatic record, in: The Tectonic and Climatic Evolution of the Arabian Sea Region, edited by: Clift, P. D., Kroon, D., Gaedicke, C., and Craig, J., 499–516, Geological Society of London, London, 2002.

Seidenglanz, A., Prange, M., Varma, V., and Schulz, M.: Ocean temperature response to idealized Gleissberg and de Vries solar cycles in a comprehensive climate model, Geophys. Res. Lett., 39, L22602, doi:10.1029/2012GL053624, 2012.

Shetye, S. R., Gouveia, A. D., and Shenoi, S.: Circulation and water masses of the Arabian Sea, Proc. Indian Acad. Sci. (Earth Planet. Sci.), 103, 107–123, 1994.

Solanki, S. K., Usoskin, I. G., Kromer, B., Schüssler, M., and Beer, J.: Unusual activity of the Sun during recent decades compared to the previous 11,000 years, Nature, 431, 1084–1087, 2004.

Southon, J., Kashgarian, M., Fontugne, M., Metivier, B., and Yim, W. W. S.: Marine Reservoir Corrections for the Indian Ocean and Southeast Asia, Radiocarbon, 44, 167–180, 2002.

Staubwasser, M., Sirocko, F., Grootes, P. M., and Erlenkeuser, H.: South Asian monsoon climate change and radiocarbon in the Arabian Sea during early and middle Holocene, Paleoceanography, 17, 15-1–15-12, 2002.

Staubwasser, M., Sirocko, F., Grootes, P. M., and Segl, M.: Climate change at the 4.2 ka BP termination of the Indus valley civilization and Holocene south Asian monsoon variability, Geophysical Res. Lett., 30, 1425, doi:10.1029/2002GL016822, 2003.

Steinhilber, F., Abreu, J. A., Beer, J., Brunner, I., Christl, M., Fischer, H., Heikkilä, U., Kubik, P. W., Mann, M., McCracken, K. G., Miller, H., Miyahara, H., Oerter, H., and Wilhelms, F.: 9,400 years of cosmic radiation and solar activity from ice cores and tree rings., P. Natl. Acad. Sci. USA, 109, 5967–5971, 2012.

Telford, R.: palaeoSig: Significance Tests of Quantitative Palaeoenvironmental Reconstructions , r package version 1.1-3 edn., 2015.

Telford, R. J. and Birks, H. J. B.: A novel method for assessing the statistical significance of quantitative reconstructions inferred from biotic assemblages, Quaternary Sci. Rev., 30, 1272–1278, 2011.

ter Braak, C. J. F. and Juggins, S.: Weighted averaging partial least squares regression (WA-PLS): An improved method for reconstructing environmental variables from species assemblages, Hydrobiologia, 269–270, 485–502, 1993.

Thamban, M., Kawahata, H., and Rao, V. P.: Indian summer monsoon variability during the holocene as recorded in sediments of the Arabian Sea: Timing and implications, J. Oceanography, 63, 1009–1020, 2007.

Tomczak, M. and Godfrey, J. S.: Regional Oceanography, Pergamon, Oxford, U.K., 1994.

Tribovillard, N., Algeo, T. J., Lyons, T., and Riboulleau, A.: Trace metals as paleoredox and paleoproductivity proxies: An update, Chem. Geol., 232, 12–32, 2006.

Turner, T. E., Swindles, G. T., Charman, D. J., Langdon, P. G., Morris, P. J., Booth, R. K., Parry, L. E., and Nichols, J. E.: Solar cycles or random processes? Evaluating solar variability in Holocene climate records, Scientific Reports, 6, 23961, doi:10.1038/srep23961, 2016.

von Rad, U., Schaaf, M., Michels, K. H., Schulz, H., Berger, W. H., and Sirocko, F.: A 5000-yr Record of Climate Change in Varved Sediments from the Oxygen Minimum Zone off Pakistan, Northeastern Arabian Sea, Quaternary Res., 51, 39–53, doi:10.1006/qres.1998.2016, 1999.

Wang, L., Sarnthein, M., Erlenkeuser, H., Grimalt, J., Grootes, P., Heilig, S., Ivanova, E., Kienast, M., Pelejero, C., and Pflaumann, U.: East Asian monsoon climate during the Late Pleistocene: high-resolution sediment records from the South China Sea, Mar. Geol., 156, 245–284, doi:10.1016/S0025-3227(98)00182-0, 1999.

Wang, Y., Cheng, H., Edwards, R. L., He, Y., Kong, X., and An, Z.: The Holocene Asian monsoon: links to solar changes and North Atlantic climate, Science, 308, 854–857, 2005.

Ward, B. B., Devol, A. H., Rich, J. J., Chang, B. X., Bulow, S. E., Naik, H., Pratihary, A., and Jayakumar, A.: Denitrification as the dominant nitrogen loss process in the Arabian Sea, Nature, 461, 78–81, 2009.

Wedepohl, K. H.: Environmental influences on the chemical composition of shales and clays, in: Physics and Chemistry of the Earth, edited by: Ahrens, L. H., Press, F., Runcorn, S. K., and Urey, H. C., 307–331, Oxford, 1971.

Wedepohl, K. H., Merian, E., Anke, M., Ihnat, M., and Stoeppler, M.: The Composition of Earth's Upper Crust, Natural Cycles of Elements, Natural Resources, p. 2, Wiley-VCH Verlag GmbH, Weinheim, 1991.

Wyrtki, K.: Physical Oceanography of the Indian Ocean, The Biology of the Indian Ocean, 18–36, 1973.

You, Y.: Intermediate water circulation and ventilation of the Indian Ocean derived from water-mass contributions, J. Mar. Res., 56, 1029–1067, 1998.

You, Y. and Tomczak, M.: Thermocline circulation and ventilation in the Indian Ocean derived from water mass analysis, Deep-Sea Res. Pt. I, 40, 13–56, 1993.

Zahn, R. and Pedersen, T. F.: Late Pleistocene evolution of surface and mid depth hydrography at the Oman Margin: planktonic and benthic isotope records at Site 724, Proc. Ocean Drilling Program, 1991.